(Received 5 March 2025, Accepted 16 April 2025, Scheduled 2 May 2025)

A Compact Quintuple-Mode Wideband Bandpass Filter Using Disk-Loaded Feeding Lines in a Single Cylindrical Cavity

Maha H. Elfeshawy[1, *], Hany F. Hammad[1], and Yasmine A. Zaghloul[2]

[1] *Faculty of Information and Engineering Technology, The German University in Cairo (GUC), Cairo, Egypt*
[2] *Electrical Engineering Department, German International University (GIU), Cairo, Egypt*

ABSTRACT: This work presents a quintuple-mode wideband bandpass filter utilizing a cylinder cavity loaded with a metallic perturbation on each base and a gap between them. The cylindrical cavity is fed with two inline disk-loaded feeding lines placed in the middle of the cavity wall. Two inline shorting pins are placed orthogonally in the same feeding lines plane. The five resonant modes are: TM_{011}, TE_{111}, the degenerate modes of TE_{211} and quasi-TE_{311} excited by the pair of disk-loaded feeding lines and shorting pins. This combination allows the generation of two transmission zeros (TZs) out of the passband. The mode analysis and geometric configuration are well studied and presented in this work. The results of the quintuple-mode filter demonstrated a fractional bandwidth of 66.87% at a central frequency of 3.69 GHz with insertion loss 0.18 dB and return loss higher than 19.4 dB. The coupling matrix of the proposed filter is synthesized as a five-pole Chebyshev filter showing close alignment with the simulated results. Finally, the proposed bandpass filter is fabricated and measured for comparison. Close agreement is achieved between the simulated and measured results.

1. INTRODUCTION

Waveguide cavity filters have been extensively utilized in wireless communication base stations, as they exhibit attributes of minimal loss of elevated power capacity and high-quality factor (Q). The new generations of mobile communications demand high data rate transmission, which relies on wide bandwidth [1]. In addition, the size of bandpass filters (BPFs) in base stations is required to be smaller to meet the demands of wireless communication system miniaturization. An approach to meet miniaturization is to change the physical structure of the resonator as in [2] through vertical integration of components such as bulk acoustic wave (BAW) filters and radio frequency silicon-on-insulator (RF-SOI) switches on a single chip, along with advanced materials like Aluminum Nitride (AlN) and Scandium-doped Aluminum Nitride (ScAlN) to enhance performance and compactness. Another approach is to change the inner cavity structure of the traditional resonator to produce additional modes in a single resonator. In such a way, one physical resonator can be modeled as a series of electrical resonators [3]. The multimode resonator (MMR) was first proposed by Lin in 1951 [4] by introducing the first quintuple-mode BPF in a single spherical cavity. Lin stated that it is possible to couple degenerate modes in a single cavity by introducing perturbations to the ideal geometric configuration of the cavity. These perturbations form a sequence of coupled circuits that form an N^{th} order filter response without using N resonators as in the traditional method, where N is a natural number. Various wideband MMR filters have been documented in the literature employing different geometric shapes and coupling elements [1, 5–21]. A class of triple-mode wideband BPFs was presented in [1] using coaxial resonators. The introduced three triple-mode BPFs operate at center frequency 2.5 GHz with 40% fractional bandwidth (FBW). Miniaturization was achieved by replacing the orthogonal feeding lines and metallic core with a pair of L-shaped feeding probes and a loading disk. Ref. [11] presented a triple-mode BPF exhibiting a FBW of 30% with a central frequency of 3.2 GHz. The triple-mode filter was realized by applying a singular offset perturbation inside a cylindrical cavity with two orthogonally arranged feeding lines. An enhancement of 1% in the FBW was achieved in this study by substituting the singular perturbation with two smaller perturbations on the cavity base. This alteration yielded a quadruple-mode BPF characterized by three TZs. The influence of the cylindrical cavity height on the positioning of the TZ is documented, indicating that an increase in the resonator height facilitates the regulation of the TZs location towards the upper band of the passband, thereby resulting in a more pronounced filtering response. A quintuple-mode BPF was realized in [12] by implementing three small metallic cylinders on the base of a cylindrical cavity and fed with two orthogonal feeding lines to obtain a 36% FBW at 3.2 GHz with four TZs in the rejection band. Ref. [13] presents a compact triple-mode BPF using cylindrical post-loaded cavity resonators fabricated via monolithic SLA-based 3D-printing. The triple-mode BPF features two TZs that can be generated below or above the passband. Two triple-mode BPFs are combined to obtain a sixth-order degree BPF that operates around 3.42 GHz with FBW near 13.3% and two TZs below and above the passband for high selectivity. A triple-mode BPF operating at 5.5 GHz with 58% FBW is presented in [14], using a single rectangular waveguide cavity excited by two adjacent feeding lines on one cavity side, achieving return loss above

* Corresponding author: Maha H. Elfeshawy (maha.elfeshawy@guc.edu.eg, maha.h.elfeshawy@gmail.com).

10 dB and insertion loss (IL) about 0.5 dB. Similarly, in [15], a triple-mode BPF is realized by loading a rectangular cavity with metallic cylinders and a circular plate to couple three TM modes, operating at 3.24 GHz with 16.1% FBW and one TZ in the upper rejection band. Ref. [16] presents a quasi-elliptic bandpass filter by embedding non-resonating mode waveguide cavities within the structure of an evanescent-mode filter. The fundamental resonator can provide a third-order filter response with a single TZ that can be located below or above the passband with 4.2% FBW at 10 GHz. Three sections are combined to create a ninth-order filter response with a wide rejection band. Ref. [17] explores the creation of a triple-mode bandpass filter utilizing a coaxial-shaped multi-mode resonator fed with two orthogonal feeding probes. The triple-mode filter achieved 1.5% FBW at 2 GHz by employing six probes, which made the structure highly frequency-sensitive and difficult to tune. In [21], a symmetric pair of perturbations were placed on a cylinder cavity base deploying a coaxial resonator with discontinuity in its metallic core to implement a quadruple-mode BPF and fed with a pair of symmetric extended conductive feeding lines. The quadruple-mode BPF has 45.5% FBW centered at 3.85 GHz and three TZs in the rejection band achieving return loss (RL) $>$ 19 dB in the passband. Ref. [22] presents a quintuple-mode wideband BPF at 5.8 GHz with 70% FBW by inserting two shorting pins and two disk-loaded feeding lines in a single rectangular cavity resonator to achieve RL $>$ 10 dB and IL $<$ 0.65 dB in the passband.

This work presents a miniaturized quintuple-mode wideband BPF that employs a cylindrical cavity that contains two metallic cylindrical perturbations coaxially and two shorting pins fed with two inline disk-loaded feeding lines. The coupling topology of the fields inside the cavity is presented along with the synthesized coupling matrix according to the theory outlined in [23–25]. This article is organized as follows. Section 2 discusses the filter mode analysis and the geometric configuration of the quadruple-mode filter. In Section 3, the coupling scheme of the quadruple-mode filter is introduced along with the matrix synthesis. Section 4 introduces the fabrication of the optimized structure and its measured results, in addition to a comparison between the proposed filter and previous work. Finally, this work is concluded in Section 5.

2. QUINTUPLE-MODE FILTER ANALYSIS

The dimensions of the cylindrical cavity resonator, a and d, shown in Fig. 1 are initially calculated using the reference mode chart for a cylindrical cavity in [26], so that $(a/d)^2$ is given by 0.89, where the diameter a can be calculated from the cut-off wavelength λ_c for an empty cylinder from Bessel's equation as:

$$\lambda_c = 3.41\,\frac{a}{2} \tag{1}$$

The resonant frequencies of *TM* and *TE* modes of order m, n, and l in a cylindrical cavity resonator can be calculated as follows [27]:

$$f_{TM_{mnl}} = \frac{c}{2\pi\sqrt{\mu_r\varepsilon_r}}\sqrt{\left(\frac{P_{mn}}{a/2}\right)^2+\left(\frac{l\pi}{d}\right)^2} \tag{2}$$

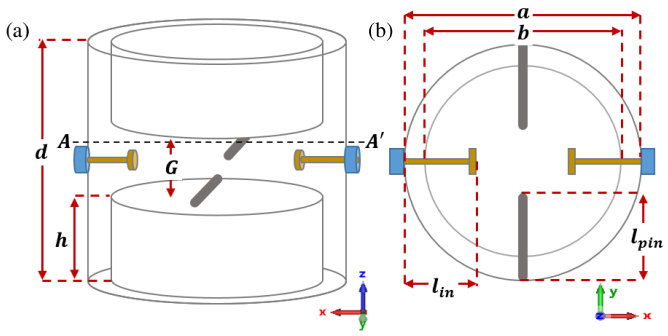

FIGURE 1. Configuration of the proposed quintuple-mode filter. (a) Three-dimensional view. (b) Top view at cut plane A-A'.

$$f_{TE_{mnl}} = \frac{c}{2\pi\sqrt{\mu_r\varepsilon_r}}\sqrt{\left(\frac{P'_{mn}}{a/2}\right)^2+\left(\frac{l\pi}{d}\right)^2} \tag{3}$$

where c is the speed of light in free space; $a/2$ is the cylinder cavity radius; μ_r and ε_r are the relative permeability and permittivity of the cavity filling material, respectively, set to 1 for an air-filled cavity; P_{mn} and P'_{mn} are the roots of the first-order Bessel function and its derivative for modes *TM* or *TE*, respectively. The cylindrical cavity is loaded with a coaxial metallic cylinder of diameter b with a gap G in the middle, forming two metallic cylindrical perturbations of height h placed symmetrically at each base of the cavity as shown in Fig. 1. However, the gap in the middle of the inner conductor cylinder plays the main role in bringing the resonant frequencies of the resonating modes near each other in the desired passband as discussed in the following subsections. The filter is fed with two coaxial feeding lines placed along x-axis. The cores of the feeding lines are extended inside the cavity with length l_{in} and loaded with small disks to strengthen coupling between modes and enhance matching. Furthermore, the cylinder cavity is loaded with a pair of shorting pins aligned along y-axis. The shorting pins and feeding lines are placed exactly in the middle of the cavity height at $d/2$. The mode analysis and the effect of the filter parameters on resonant mode frequencies are discussed in the following subsections. All simulations in this work are conducted using CST Studio (EM simulation software).

2.1. Mode Analysis

Fig. 2 is presented to understand the coupling scheme among the disk-loaded feeding lines, shorting-pins, and resonant modes. As mentioned in [28], the feeding probe couples to the electric field perpendicular to the cavity wall at the probe location. The closer the probe is to a field maximum, the stronger the obtained coupling is. Normally, the length of an unloaded probe is equal to a quarter wavelength, which leads to the input impedance nearly equivalent to that of an open circuit [28]. In the proposed filter, the two disk-loaded feeding lines placed on the x-axis introduce energy into the cavity. The feeding configuration should align with the mode field structure for efficient coupling. Most of the cylinder cavity filters reported in the literature introduced mode TM_{010} as the first resonating mode as it has the least resonant frequency. The TM_{010} mode has an electric field E that is purely axial (E_z) and does not

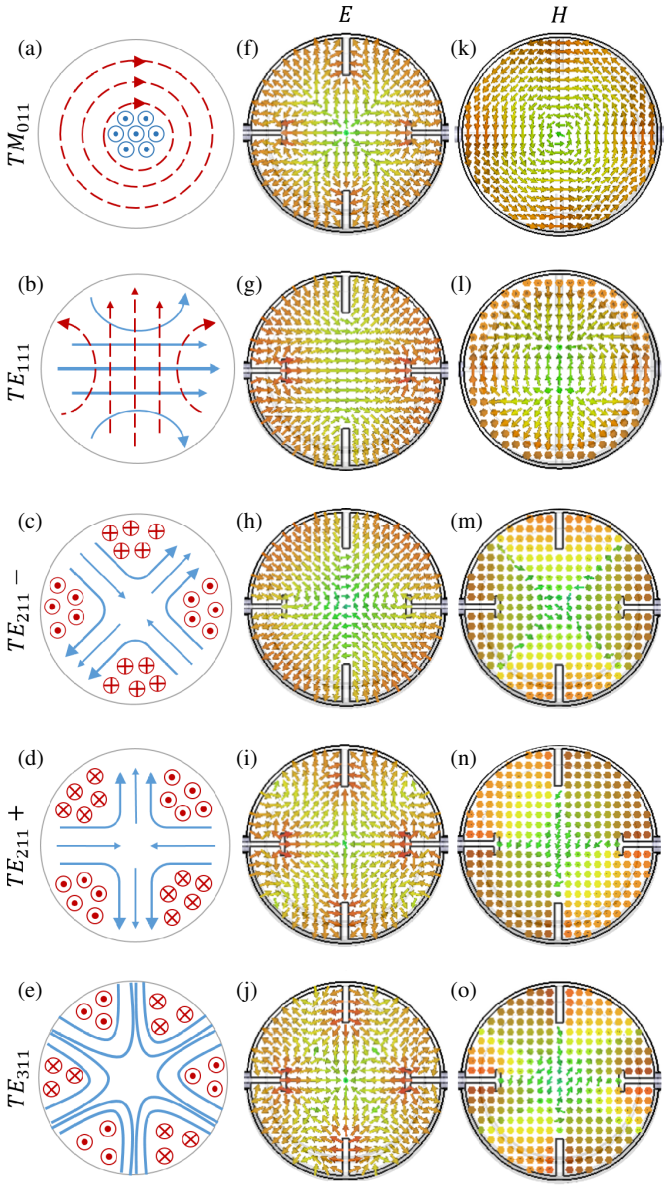

FIGURE 2. Field distributions of the five resonant modes: (a)–(e) electric fields in blue solid lines and magnetic field in red dashed lines, (f)–(j) simulated electric field distribution at cross-section plane $d/2$, simulated magnetic field distribution (k)–(l) at cross-section plane A-A' and (m)–(o) at cross-section plane at $d/2$.

vary in the transverse plane. In contrast, the magnetic field H is purely transverse, with dominating H_ϕ. The TM_{010} mode has no significant field variation along the x-axis, making it difficult for coaxial feeds placed in this direction to excite the mode efficiently. However, placing the feeding lines in the middle of the cavity provides sufficient coupling with mode TM_{011} having phase change in its electric field exactly at the center of the cavity height as shown in Fig. 2(f). Fig. 2(k) shows the magnetic field distribution of mode TM_{011} at plane A-A' above the middle of the height, which is similar to that of mode TM_{010}. Fig. 2(a) shows the reference electric and magnetic field distributions of mode TM_{011} away from the center of the cavity height. The reference field distributions of the four TE modes TE_{111}, degenerates of TE_{211} and TE_{311} in the transverse plane are declared in Figs. 2(b)–(e). In-phase feeding lines allow strong electric coupling with one component of degenerates of TE_{111} mode that has its electric field aligned with the feeding lines as shown in Fig. 2(g). Similarly, mode $TE_{211}+$ shown in Fig. 2(i) is excited by the two in-phase feeding lines. While the two shorting pins aligned along y-axis along with the feeding probes allow cross-coupling between TE_{111} and $TE_{211}+$ that yield the resonance of $TE_{211}-$ shown in Fig. 2(h). Furthermore, the configuration of the shorting pins and feeding lines allows the excitation of the fifth mode in the passband. By observing its field distributions in Figs. 2(j) and (o), it is found to be a quasi-TE_{311}, where it has three variations in the azimuth direction (ϕ). While the degenerate mode TE_{311} is not excited, it forms the TZ located in the upper rejection band. The following subsection introduces the effect of the perturbation dimensions on the resonant frequencies of the five resonating modes and the effect of the disk-loaded feeding lines and shorting pins on the filter frequency response.

2.2. Geometric Configuration

As the resonant frequencies of the five modes TM_{011}, TE_{111}, two degenerates of TE_{211} and TE_{311} are controlled by the perturbation size, shorting pins length, and disk-loaded feeding probe size, a full analysis is conducted on each of the parameters separately. First, the effect of the gap between the perturbations G is related to the height of the perturbations h as $(d-2h)$. Enlarging the gap in the middle of the metallic core affects the distribution of the electromagnetic fields within the cavity. This changes the effective length of the cavity for the resonating modes and shifts their resonance frequencies to higher values [29] as presented in Fig. 3. The height of the two perturbations is set to be the same as that recommended in [17]. At higher values of G, the resonant frequencies of mode $TE_{211}-$ and mode TE_{311} approach higher frequencies outside the desired passband, which leads to a lower-order filter response. Fig. 4 shows the S_{21} frequency response at different values of G, where increasing the value of G moves the lower TZ towards the passband and reduces the passband BW.

Second, the effect of the diameter of the perturbation b on the five resonating modes is presented in Fig. 5. The perturbation diameter plays a main role in controlling the sharpness of the

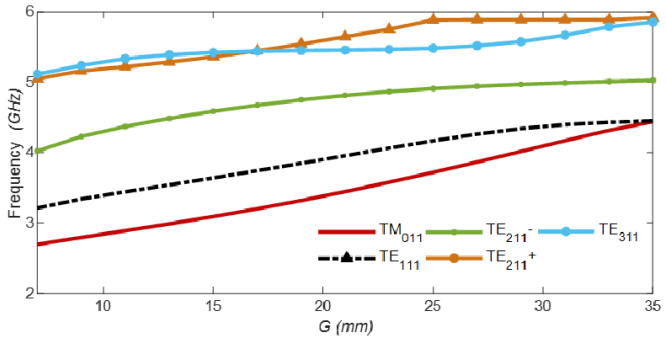

FIGURE 3. Variation of the resonant frequency of five resonant modes against the gap between the perturbations G.

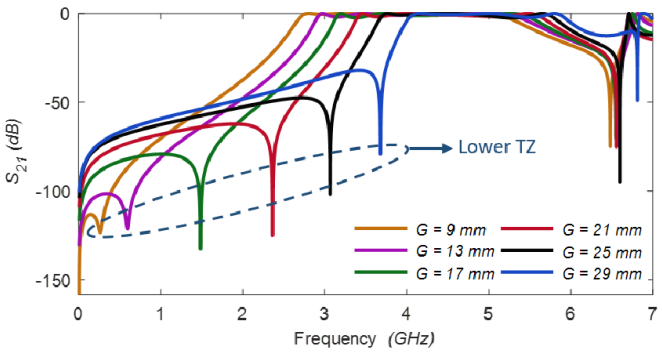

FIGURE 4. Frequency response of S_{21} at different values of the gap between the perturbations G.

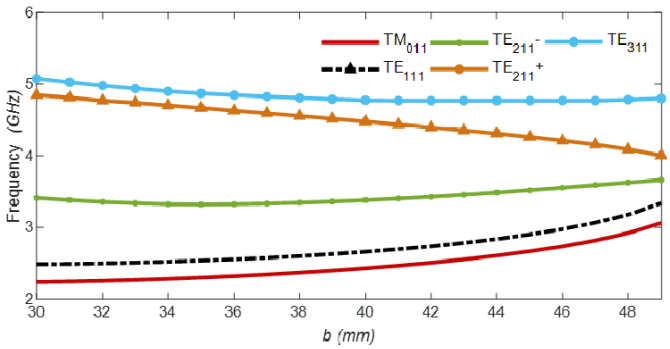

FIGURE 5. Variation of the resonant frequency of five resonant modes against the perturbations diameter b.

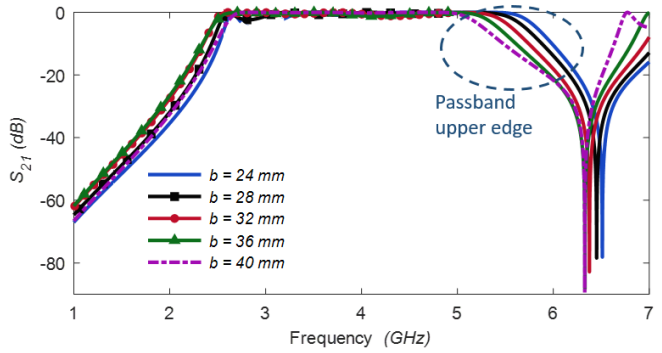

FIGURE 6. Frequency response of S_{21} at different values of perturbations diameter b.

passband upper edge. Fig. 6 shows the S_{21} frequency response at different values of b. As the value of b increases, the upper rejection band TZ slightly shifts towards the passband, while the passband upper edge roll-off increases.

2.3. Feeding and Tuning Probes

Besides perturbation dimensions, disk-loaded feeding lines are employed in cavity filters to enhance coupling efficiency, impedance matching, and hence field distribution. The external quality factors Q_e of the resonant modes are extracted against the feeding probe length l_{in} and loading disk diameter D_{disk} and presented in Fig. 7. Fig. 8 shows the S_{11} frequency response at different values of l_{in} and D_{disk} at which the

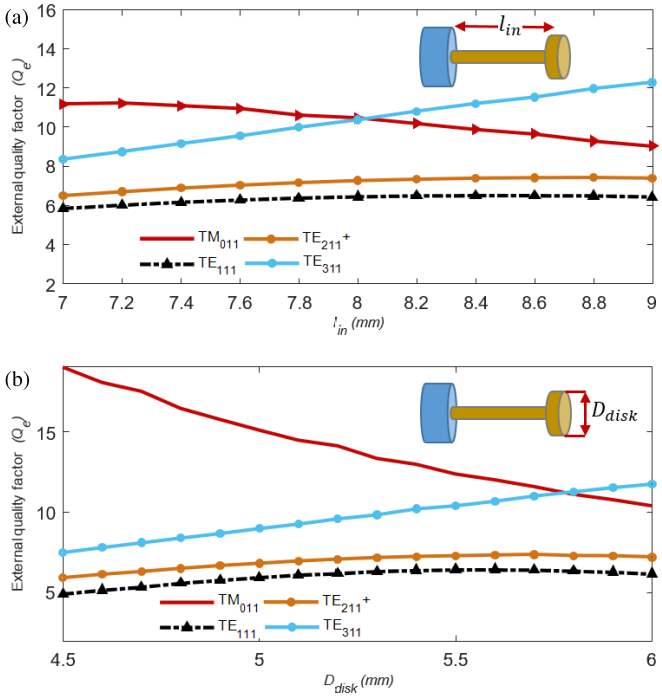

FIGURE 7. Variation of the external quality factors against (a) feeding probe length (l_{in}) and (b) loading disk diameter (D_{disk}).

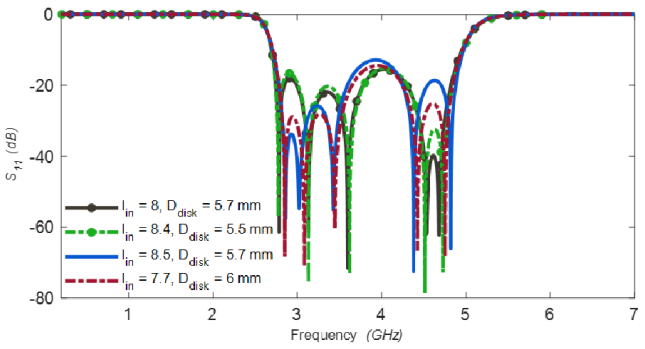

FIGURE 8. Frequency response of S_{11} at different values of feeding probe length l_{in} and loading disk diameter D_{disk}.

matching in the passband is achieved. The values of l_{in} and D_{disk} are chosen to achieve the lowest ripple level with a reasonable quality factor.

Furthermore, the length of the shorting pins l_{pin} enhances the cross-coupling between TE_{111} and $TE_{211}+$ modes to excite mode $TE_{211}-$. Fig. 9 shows the S_{11} frequency response at different values of l_{pin} and shows the effect of increasing the value of l_{pin} on shifting the upper TZ towards the rejection band. The unloaded quality factors of the five resonant modes are extracted: 2197, 2357, 2307, 2213, and 4349, respectively.

3. COUPLING MATRIX ANALYSIS

By observing the field distribution in Fig. 2, the source and load excite the four modes TM_{011}, TE_{111}, $TE_{211}+$ and quasi-TE_{311} that have their EF aligned with the source/load probes, while the two shorting pins enhance the cross-coupling be-

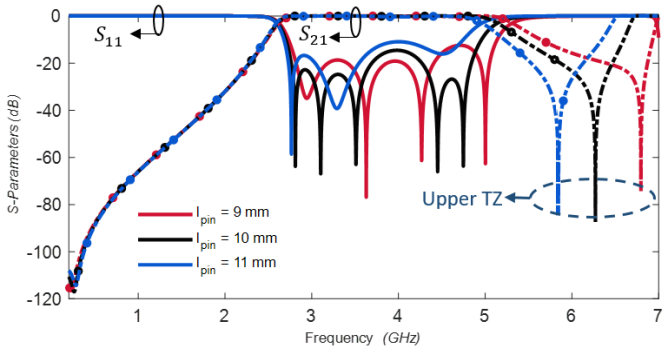

FIGURE 9. Frequency response of S_{21} at different values of shorting pins length (l_{pin}).

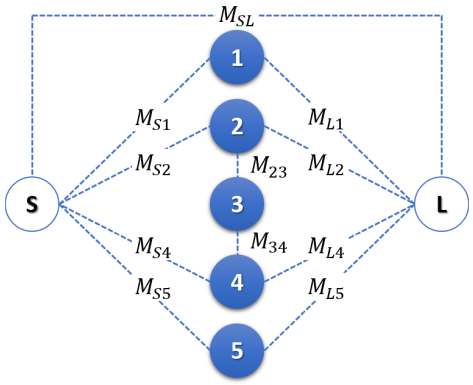

FIGURE 10. Proposed quintuple-mode filter coupling scheme.

tween TE_{111} mode $TE_{211}+$ to allow the presence of mode $TE_{211}-$ [22]. Fig. 10 shows the suggested coupling topology for the proposed quintuple PBF, and the corresponding $N+2$ general coupling matrix can be expressed as [22]:

$$\begin{bmatrix} 0 & M_{S1} & M_{S2} & 0 & M_{S4} & M_{S5} & M_{SL} \\ M_{S1} & M_{11} & 0 & 0 & 0 & 0 & M_{L1} \\ M_{S2} & 0 & M_{22} & M_{32} & 0 & 0 & M_{L2} \\ 0 & 0 & M_{32} & M_{33} & M_{34} & 0 & 0 \\ M_{S4} & 0 & 0 & M_{34} & M_{44} & 0 & M_{L4} \\ M_{S5} & 0 & 0 & 0 & 0 & M_{55} & M_{L5} \\ M_{SL} & M_{L1} & M_{L2} & 0 & M_{L4} & M_{L5} & 0 \end{bmatrix} \tag{4}$$

where M_{Si} and M_{Li} are the coupling coefficients of the i^{th} mode with the source and load, respectively; M_{ii} is the self-resonance of the i^{th} mode for $i = 1, 2, 3, 4, 5$; M_{ij} is the cross-coupling coefficients for $i \neq j$; M_{SL} is the source/load coupling coefficient as there could be a weak coupling between the inline feeding probes. To calculate the coupling matrix coefficient, the group delay of $|S_{11}|$ is extracted at resonant with a single feeding port. The external quality factor (Q_{ei}) for the i^{th} mode can be calculated as [30]:

$$Q_{ei} = \frac{\pi f_i \tau_i}{2} \tag{5}$$

where f_i and τ_i are the resonant frequency and group delay of the i^{th} resonant mode, respectively. The values of Q_{ei} are used to calculate the coupling coefficients M_{Si} as [25]:

$$M_{Si} = \sqrt{1/FBW \times Q_{ei}} \tag{6}$$

The self-coupling coefficients M_{ii} can be calculated as:

$$M_{ii} = \frac{f_o^2 - f_i^2}{f_i \cdot BW} \tag{7}$$

where f_o is the filter center frequency, and BW is the filter bandwidth. The positive and negative signs of M_{ii} indicate the resonances below and above f_o, respectively. The cross-coupling coefficients M_{ij} are calculated as:

$$M_{ij} = \frac{CBW_{ij}}{BW} \tag{8}$$

where CBW_{ij} is the coupling bandwidth between mode i and mode j, extracted from the eigenmode values. Finally, the source/load coupling coefficient M_{SL} can be calculated from [26]:

$$M_{SL} = \sqrt{1/Q_S \times Q_L} \tag{9}$$

where Q_S and Q_L are derived from (5) at the passband center frequency. The calculated value of M_{SL} is 2.8×10^{-10} which can be neglected. According to the filter synthesis theory outlined in [25], the source and load terminals coupled to multi-modes can generate TZs by setting two pairs of M_{Si} and M_{Li} opposite in sign. The proposed quintuple-mode BPF provides one TZ in the lower rejection band and one TZ in the upper rejection band. By observing the field distribution in Fig. 2, both modes TM_{011} and TE_{211} are symmetric with respect to the feeding probes, while modes TE_{111} and TE_{311} are asymmetric. Thus, the values of the coupling coefficients are set as $M_{S1} = M_{L1}$, $M_{S2} = -M_{L2}$, $M_{S4} = M_{L4}$, and $M_{S5} = -M_{L5}$. The extracted Q_{ei} are $Q_{S1} = 12.33$, $Q_{S2} = 6.406$, $Q_{S4} = 6.166$, and $Q_{S5} = 10.84$. The derived normalized coupling matrix is:

$$\begin{bmatrix} 0 & 0.386 & 0.51 & 0 & 0.492 & 0.412 & 0 \\ 0.386 & 1.129 & 0 & 0 & 0 & 0 & 0.386 \\ -0.51 & 0 & 0.519 & 0.13 & 0 & 0 & 0.51 \\ 0 & 0 & 0.13 & 0.057 & -0.18 & 0 & 0 \\ 0.492 & 0 & 0 & -0.18 & -0.44 & 0 & 0.492 \\ -0.412 & 0 & 0 & 0 & 0 & -1.125 & 0.412 \\ 0 & 0.386 & 0.51 & 0 & 0.492 & 0.412 & 0 \end{bmatrix} \tag{10}$$

The proposed quintuple-mode BPF coupling matrix can be synthesized for a Chebyshev filter with FBW 66.87% at center frequency 3.69 GHz and 20 dB return loss from 2.8 GHz to 4.785 GHz. Two TZs are located out of the passband at 0.134 GHz and 6.29 GHz. To ensure the filter response, the proposed filter is simulated using HFSS software with an evaluation license. A comparison between the electromagnetic (EM) simulated responses using both CST and HFSS along with the synthesis technique by coupling matrix is depicted in Fig. 11. The simulated S_{11} shows close agreement with the theoretically synthesized response. The simulated and synthesized S_{21} have the same TZs locations.

TABLE 1. Comparisons with other reported cylindrical multimode wideband BPFs.

Ref.	N	f_o (GHz)	FBW (%)	TZ's	IL (dB)	RL (dB)	Size (diameter × height)	Q_u
[1] I	3	2.5	40	2	0.28	> 17.5	$\phi 0.46\lambda_g \times 0.19\lambda_g$	1284
[1] II	3	2.5	40	2	0.32	> 16	$\phi 0.28\lambda_g \times 0.21\lambda_g$	1376
[1] III	3	2.5	40	3	0.34	> 20	$\phi 0.26\lambda_g \times 0.115\lambda_g$	1283
[10]	4	2.2	45	3	0.4	> 15	$\phi 0.27\lambda_g \times 0.16\lambda_g$	1820
[11] I	3	3.2	30	2	0.5	> 15	$\phi 0.5\lambda_g \times 0.5\lambda_g$	4672
[11] II	4	3.3	31	3	0.5	> 15	$\phi 0.5\lambda_g \times 0.5\lambda_g$	4654
[12]	5	3.2	36	4	0.5	> 10	$\phi 0.53\lambda_g \times 0.54\lambda_g$	4375
[21]	4	3.85	45.55	3	0.5	> 19	$\phi 0.6\lambda_g \times 0.88\lambda_g$	2286
T.W.	**5**	**3.69**	**66.87**	**2**	**0.18**	$\mathbf{> 23.5}$	$\boldsymbol{\phi 0.61\lambda_g \times 0.65\lambda_g}$	**2197**

T.W. — this work; N — filter order; f_o — center frequency; FBW — fractional bandwidth; IL — insertion loss; RL — return loss; λ_g — guided wavelength; Q_u — unloaded quality factor.

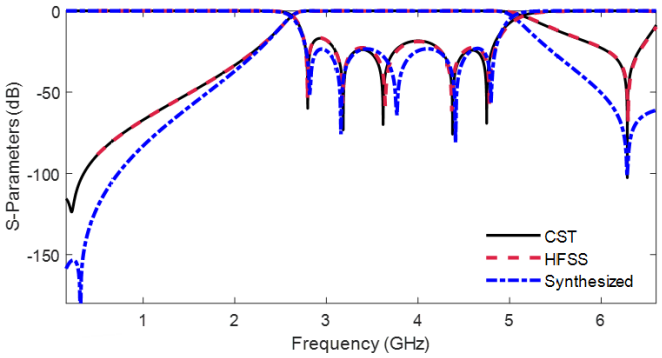

FIGURE 11. S-parameters for the EM simulated response and the synthesis technique.

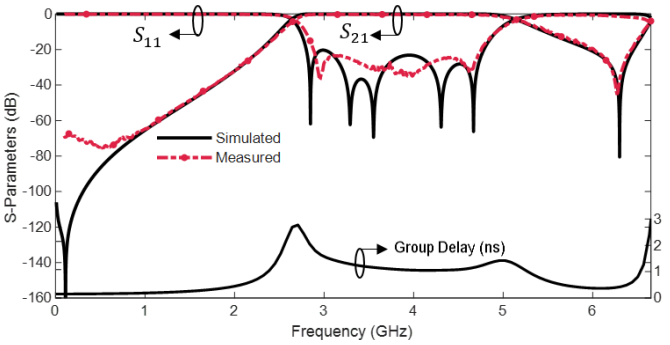

FIGURE 13. Simulated and measured S-parameters of the proposed quintuple-mode BPF.

4. FABRICATION AND MEASURED RESULTS

The proposed quintuple-mode BPF is fabricated from Aluminum 7075 ($\sigma = 1.94 \times 10^7$ S/m) using milling machining technology. To ease the fabrication process, the prototype is divided into two identical parts as shown in Fig. 12 and assembled using fixing pins. The two 50-ohm extended feeding lines are joined to the loading disk,s and two shorting pins are placed orthogonal to the disk-loaded feeding lines. The final optimized dimensions of the proposed filter are: $a = 50$, $d = 53$, $b = 41.6$, $h = 22.5$, $D_{disk} = 6$, $l_{pin} = 10$, $l_{in} = 6.6$ (all in mm). The measured results are compared to the simulated ones in Fig. 13. The simulated FBW is 67.98% at 3.68 GHz while the measured FBW is 66.87% at 3.69 GHz. The measured RL is more than 23.5 dB over the whole passband, and the passband measured IL is less than 0.18 dB. The lower rejection band is below -20 dB below 2.37 GHz, and the upper rejection band is below -20 dB from 5.72 GHz to 6.37 GHz with a TZ at 6.16 GHz. The proposed quintuple-mode BPF exhibits an average group delay of 0.5 ns across the passband. Table 1 presents a comparison between the proposed quintuple-mode BPF and the cylindrical multimode BPFs previously reported in the literature, showing the merits of the proposed design in terms of FBW, IL, RL, and compact size.

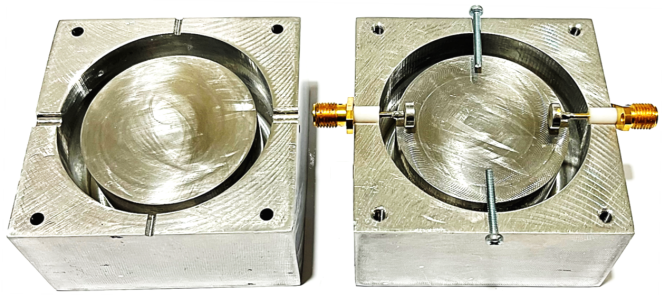

FIGURE 12. The fabricated prototype of the proposed quintuple-mode BPF.

5. CONCLUSION

This article has presented the implementation of a compact quintuple-mode wideband BPF using a single metallic cylindrical cavity that employs a coaxial metallic cylinder with a gap in the middle. The five resonant modes are excited by two inline disk-loaded coaxial cables in the middle of the cavity and two shoring pins placed orthogonal to the feeding lines. This study details the derivation of the coupling scheme between the modes and the synthesis of the coupling matrix based on mode analysis and the described geometric configuration. The proposed quintuple-mode BPF operates at 3.69 GHz with 66.86% FBW with two TZs in the rejection band. The low variation in

group delay ensures high-fidelity signal transmission suitable for high-speed communication systems. The measured results closely align with the responses from electromagnetic simulation tools and synthesized data. The proposed filter presents an effective solution to achieve wide passband, high return loss, and compact design. It is well suited for applications in high-data-rate wireless communication systems.

ACKNOWLEDGEMENT

The authors would like to acknowledge the Industrial Park at The German University in Cairo (GUC) for the time and effort spent on fabricating the designed RF filter. Additionally, the authors would like to acknowledge Fluid Codes, Ansys Channel Partner, for providing an evaluation license.

REFERENCES

[1] Zhang, Z.-C., X.-Z. Yu, S.-W. Wong, B.-X. Zhao, J.-Y. Lin, X. Zhang, and K.-W. Tam, "Miniaturization of triple-mode wideband bandpass filters," *IEEE Transactions on Components, Packaging and Manufacturing Technology*, Vol. 12, No. 8, 1368–1374, Aug. 2022.

[2] Campanella, H., Y. Qian, C. O. Romero, J. S. Wong, J. Giner, and R. Kumar, "Monolithic multiband MEMS RF front-end module for 5G mobile," *Journal of Microelectromechanical Systems*, Vol. 30, No. 1, 72–80, 2021.

[3] Watanabe, A. O., M. Ali, S. Y. B. Sayeed, R. R. Tummala, and M. R. Pulugurtha, "A review of 5G front-end systems package integration," *IEEE Transactions on Components, Packaging and Manufacturing Technology*, Vol. 11, No. 1, 118–133, 2021.

[4] Lin, W.-G., "Microwave filters employing a single cavity excited in more than one mode," *Journal of Applied Physics*, Vol. 22, No. 8, 989–1001, Aug. 1951.

[5] Hameed, M., G. Xiao, and C. Xiong, "Triple-mode wideband bandpass filter using triangular waveguide cavity," in *2018 IEEE MTT-S International Wireless Symposium (IWS)*, 1–3, Chengdu, China, 2018.

[6] Liang, X.-P., K. A. Zaki, and A. E. Atia, "Dual mode coupling by square corner cut in resonators and filters," in *IEEE Transactions on Microwave Theory and Techniques*, Vol. 40, No. 12, 2294–2302, Dec. 1992.

[7] Bastioli, S., C. Tomassoni, and R. Sorrentino, "A new class of waveguide dual-mode filters using TM and nonresonating modes," *IEEE Transactions on Microwave Theory and Techniques*, Vol. 58, No. 12, 3909–3917, Dec. 2010.

[8] Feng, S.-F., S.-W. Wong, F. Deng, L. Zhu, and Q.-X. Chu, "Triple-mode wideband bandpass filter using single rectangular waveguide cavity," in *2016 IEEE International Conference on Computational Electromagnetics (ICCEM)*, 287–289, Guangzhou, China, 2016.

[9] Zhao, K. and D. Psychogiou, "Monolithic SLA-based capacitively-loaded high-Q coaxial resonators and bandpass filters," in *2020 50th European Microwave Conference (EuMC)*, 471–474, Utrecht, Netherlands, 2021.

[10] Zhang, Z.-C., S.-W. Wong, X. Yu, B. Zhao, D. Wang, and R. Chen, "Compact quadruple-mode wideband bandpass filter using L-shaped feed-line in a single cavity," *IEEE Microwave and Wireless Components Letters*, Vol. 31, No. 10, 1111–1114, Oct. 2021.

[11] Wong, S.-W., S.-F. Feng, L. Zhu, and Q.-X. Chu, "Triple- and quadruple-mode wideband bandpass filter using simple perturbation in single metal cavity," *IEEE Transactions on Microwave Theory and Techniques*, Vol. 63, No. 10, 3416–3424, Oct. 2015.

[12] Wong, S.-W., S.-F. Feng, F. Deng, L. Zhu, and Q.-X. Chu, "A quintuple-mode wideband bandpass filter on single metallic cavity with perturbation cylinders," *IEEE Microwave and Wireless Components Letters*, Vol. 26, No. 12, 975–977, Dec. 2016.

[13] Zhao, K. and D. Psychogiou, "Additively manufactured and monolithically-integrated triple-mode post-loaded cavity-resonator-based bandpass filters," *IEEE Journal of Microwaves*, Vol. 3, No. 4, 1237–1247, 2023.

[14] Feng, S.-F., S.-W. Wong, L. Zhu, and Q.-X. Chu, "A triple-mode wideband bandpass filter using single rectangular waveguide cavity," *IEEE Microwave and Wireless Components Letters*, Vol. 27, No. 2, 117–119, Feb. 2017.

[15] Li, Y.-Q., J. Xu, X. Liu, J. Li, and D.-S. La, "A wideband bandpass cavity filter using three TM modes," in *2024 International Conference on Microwave and Millimeter Wave Technology (ICMMT)*, Vol. 1, 1–3, Beijing, China, 2024.

[16] Bastioli, S. and R. V. Snyder, "Quasi-elliptic evanescent-mode filters using non-resonating mode waveguide cavities," *International Journal of Microwave and Wireless Technologies*, Vol. 7, No. 3–4, 211–218, 2015.

[17] Yakuno, S. and T. Ishizaki, "Novel cavity-type multi-mode filter using TEM-mode and TE-mode," in *2012 Asia Pacific Microwave Conference Proceedings*, 376–378, Kaohsiung, Taiwan, 2012.

[18] Lai, S.-L. and W.-G. Lin, "A five mode single spherical cavity microwave filter," in *1992 IEEE MTT-S Microwave Symposium Digest*, 909–912, Albuquerque, NM, USA, 1992.

[19] Li, J., Z. Chen, and T. Yuan, "Optimized design of a miniaturized irregular spherical resonator with enhanced subtractive/additive manufacturing process compatibility," in *2020 IEEE MTT-S International Wireless Symposium (IWS)*, 1–3, Shanghai, China, 2020.

[20] Morán-López, A., J. Córcoles, J. A. Ruiz-Cruz, J. R. Montejo-Garai, and J. M. Rebollar, "Dual-mode filters in equilateral triangular waveguides with wide spurious-free response," in *2017 IEEE MTT-S International Microwave Symposium (IMS)*, 1192–1195, Honolulu, HI, USA, 2017.

[21] Elfeshawy, M. H., Y. A. Zaghloul, and H. F. Hammad, "Quadruple-mode wideband bandpass filter using symmetric structure in single cylindrical cavity," in *2023 International Microwave and Antenna Symposium (IMAS)*, 150–153, Cairo, Egypt, 2023.

[22] Wong, S.-W., S.-F. Feng, F. Deng, L. Zhu, and Q.-X. Chu, "A quintuple-mode wideband bandpass filter on single metallic cavity with perturbation cylinders," *IEEE Microwave and Wireless Components Letters*, Vol. 26, No. 12, 975–977, 2016.

[23] Szydlowski, L., A. Lamecki, and M. Mrozowski, "A novel coupling matrix synthesis technique for generalized Chebyshev filters with resonant source-load connection," *IEEE Transactions on Microwave Theory and Techniques*, Vol. 61, No. 10, 3568–3577, Oct. 2013.

[24] Uhm, M., J. Lee, I. Yom, and J. Kim, "General coupling matrix synthesis method for microwave resonator filters of arbitrary topology," *ETRI Journal*, Vol. 28, No. 2, 223–226, 2006.

[25] Cameron, R. J., "Advanced coupling matrix synthesis techniques for microwave filters," *IEEE Transactions on Microwave Theory and Techniques*, Vol. 51, No. 1, 1–10, Jan. 2003.

[26] Cameron, R. J., C. M. Kudsia, and R. R. Mansour, *Microwave Filters for Communication Systems: Fundamentals, Design, and Applications*, 2nd ed., John Wiley & Sons, 2018.

[27] Pozar, D. M., *Microwave Engineering*, 4th ed., Wiley, New York, NY, USA, 2011.

[28] Collin, R. E., *Field Theory of Guided Waves*, 2nd ed., John Wiley & Sons, New York, 1991.

[29] Wells, C. G. and J. A. R. Ball, "Gap capacitance of a coaxial resonator using simplified mode matching," *IEE Proceedings — Microwaves, Antennas and Propagation*, Vol. 151, No. 5, 399–403, 2004.

[30] Squillaci, M. and J. Perelaer, *Advanced Materials and Technologies*, 191–234, John Wiley & Sons, 2001.